Crystal Structure of Histidine Ammonia-Lyase Revealing a Novel Polypeptide Modification as the Catalytic Electrophile[†,‡]

Torsten F. Schwede,[§] János Rétey,[||] and Georg E. Schulz*[,§]

Institut für Organische Chemie und Biochemie, Albert-Ludwigs-Universität, Albertstrasse 21, D-79104 Freiburg im Breisgau, Germany, and Institut für Organische Chemie, Lehrstuhl Biochemie der Universität, Richard-Willstätter-Allee, Universität Karlsruhe, D-76128 Karlsruhe, Germany

Received December 14, 1998; Revised Manuscript Received February 3, 1999

ABSTRACT: Histidine ammonia-lyase (EC 4.3.1.3) catalyzes the nonoxidative elimination of the α-amino group of histidine and is closely related to the important plant enzyme phenylalanine ammonia-lyase. The crystal structure of histidase from *Pseudomonas putida* was determined at 2.1 Å resolution revealing a homotetramer with D_2 symmetry, the molecular center of which is formed by 20 nearly parallel α-helices. The chain fold, but not the sequence, resembles those of fumarase C and related proteins. The structure shows that the reactive electrophile is a 4-methylidene-imidazole-5-one, which is formed autocatalytically by cyclization and dehydration of residues 142−144 with the sequence Ala-Ser-Gly. With respect to the first dehydration step, this modification resembles the chromophore of the green fluorescent protein. The active center is clearly established by the modification and by mutations. The observed geometry allowed us to model the bound substrate at a high confidence level. A reaction mechanism is proposed.

Amino acid degradation starts in most cases with the oxidative removal of the α-amino group catalyzed by transaminases and resulting in α-keto acids. The degradation of histidine to glutamate, however, follows a different pathway. In the first step catalyzed by histidine ammonia-lyase (histidase, EC 4.3.1.3), the α-amino group elimination results in the α−β-unsaturated *trans*-urocanate (Scheme 1). Urocanate has been suggested to function as a sun blocker in human skin (*1*). Histidase failure in humans is known as the disease histidinemia (*2*).

The catalyzed elimination reaction is a chemical challenge because the enzyme has to abstract a nonacidic proton from the substrate C_β atom neighboring the highly acidic α-ammonium group, which must remain protonated to provide a good leaving group. The same reaction mechanism has been suggested for the homologous (19−29% sequence identity) enzyme phenylalanine ammonia-lyase from plants (EC 4.3.1.5) (*3*, *4*), which produces cinnamic acid as the precursor of lignins, coumarins, and flavonoids (*5*).

The deamination reaction catalyzed by these two enzymes requires an electrophilic group. On the basis of chemical modification experiments (*6*, *7*) and mutational studies (*8*, *9*), this group was proposed to be a dehydroalanine residue that is formed autocatalytically from a serine, here from Ser143. Dehydroalanine is only very rarely observed like, e.g., in peptide antibiotics such as nisin (*10*), or as a result of side chain eliminations in proteins (*11*, *12*). We present here the structure of histidase at 2.1 Å resolution, establishing a polypeptide modification that forms a novel catalytically essential electrophilic group.

Scheme 1

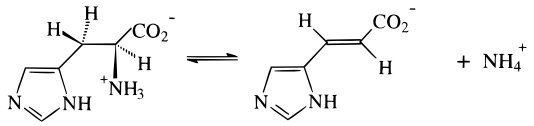

Table 1: Data Collection and MIR Phasing Statistics

	Native-A	MMA	CIP	Native-B
space group	$P2_1$	$P2_1$	$P2_1$	$I222$
resolution (Å)	38−2.6	28−2.8	34−4.0	39−2.1
total no. of observations	141380	133653	44660	82830
no. of unique reflections	58970	46749	19386	28972
completeness (%)[a]	79 (59)	76 (72)	94 (90)	83 (66)
average $I/\sigma(I)$[a]	8.4 (3.8)	10.9 (8.4)	8.6 (10.7)	7.9 (3.0)
redundancy, overall[a]	2.4 (1.4)	2.9 (1.9)	2.3 (1.6)	2.9 (1.6)
R_{sym} (%)[a,b]	7.8 (18.1)	5.4 (8.2)	5.6 (6.5)	8.2 (18.2)
R_{iso}[c]	−	22.5	17.1	−
no. of sites	−	19	14	−
phasing power[d]	−	2.0	1.0	−

[a] Values for the outermost shell are given in parentheses. [b] $R_{sym} = \sum_{hi}|I_{hi} - \langle I_h\rangle|/\sum_{hi}I_{hi}$, where i counts through symmetry-related reflections h. [c] $R_{iso} = \sum_h|F_{PH} - F_P|/\sum_h F_{PH}$, where F_{PH} and F_P are the derivative and native structure amplitudes, respectively. [d] In the resolution range of 28−4.0 Å.

MATERIALS AND METHODS

Enzyme Production and Assay. Histidase from *Pseudomonas putida* (*13*) was expressed in *Escherichia coli* (*14*) and purified by fractionated ammonium sulfate precipitation, ion exchange chromatography (Q-Sepharose), and gel permeation chromatography (Superdex-200) (*8*). The enzyme activity

[†] The project was supported by the Graduiertenkolleg "Strukturbildung in makromolekularen Systemen", the Deutsche Forschungsgemeinschaft, and the Fonds der Chemischen Industrie.

[‡] The coordinates and structure factors are deposited with the Brookhaven Protein Data Bank as file 1B8F.

* Corresponding author. Phone: +49-761-203-6058. Fax: +49-761-203-6161. E-mail: schulz@bio.chemie.uni-freiburg.de.

[§] Albert-Ludwigs-Universität.

[||] Universität Karlsruhe.

10.1021/bi982929q CCC: $18.00
Published on Web 04/03/1999

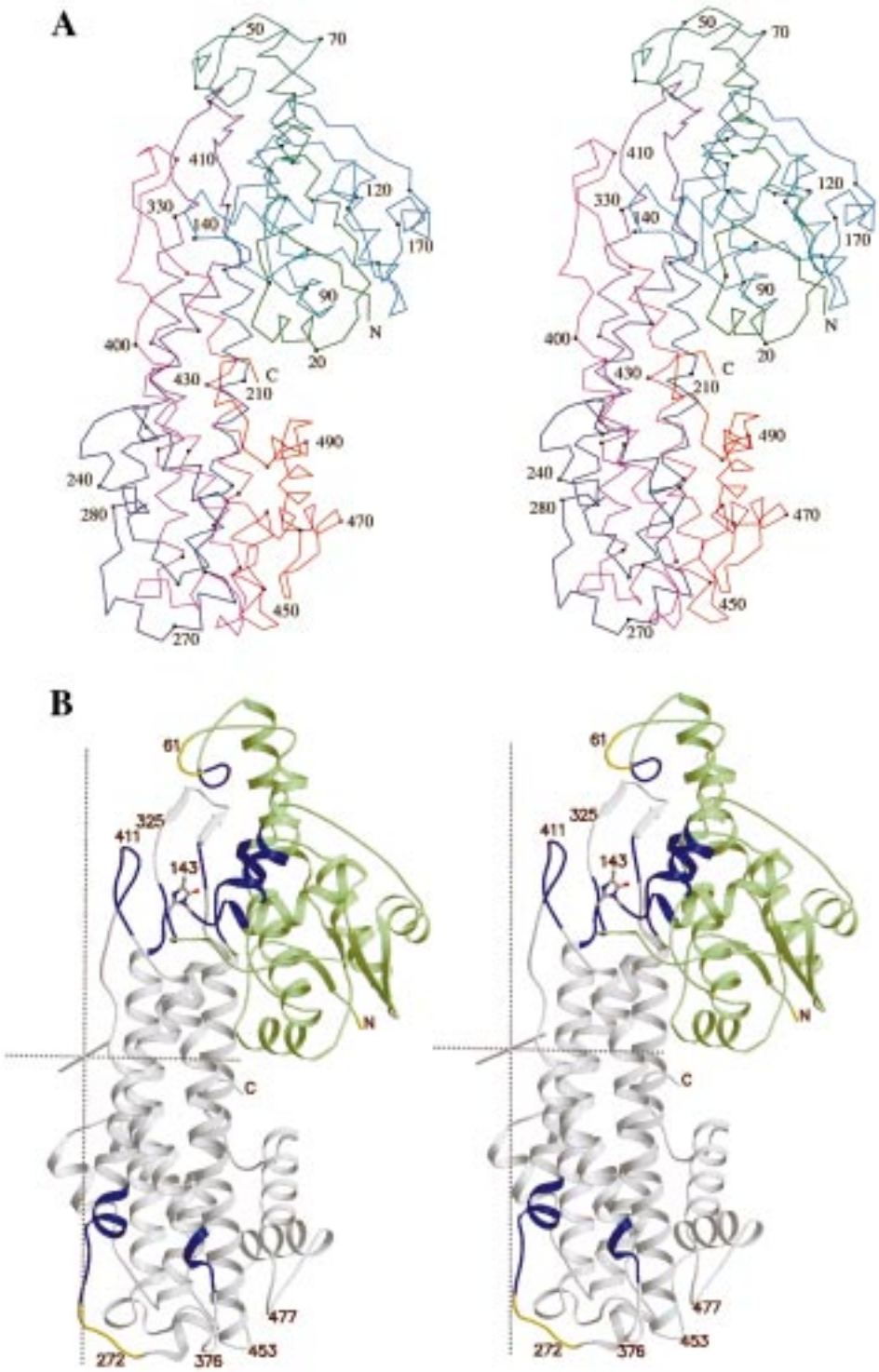

FIGURE 1: Stereoview of a histidase subunit chain fold. (A) C_α plot using a color gradient along the chain with dots at every tenth residue; some dots are labeled. (B) Ribbon plot with the N-terminal (residues 1−198, green) and C-terminal domain (gray). The modified loop containing 4-methylidene-imidazole-5-one (MIO, ball-and-stick model) is surrounded by residues (blue) from the same subunit and from two other subunits. Two segments have weak electron density (yellow). The molecular 2-fold axes are indicated.

was determined as the rate of urocanate formation measured spectrophotometrically at 277 nm (*15*). For a standard assay (*8*), the enzyme was preincubated at 25 °C for 5 min in a buffer containing 2.5 mL of 0.1 M pyrophosphate (pH 9.3), 10 μM $ZnCl_2$, and 2 mM glutathione. The reaction was started by adding 200 μL of a 0.5 M histidine solution.

Crystallization and Data Collection. Crystals of histidase mutant Cys273 → Ala (*16*) were grown by the hanging drop vapor diffusion method from a 1:1 mixture of 14 mg/mL protein with a reservoir solution [2.0 M $(NH_4)_2SO_4$, 1% glycerol, 2% PEG-400, and 0.1 M HEPES (pH 8.1)]. Data were collected using CuKα radiation from a rotation anode (Rigaku, model RU200B). Data sets Native-A, CIP, and Native-B were collected with a multiwire detector (Siemens, model X-1000) and processed with the program XDS (*17*); data set MMA was collected with an imaging plate (MAR-research, model 30-cm) and processed with the program MOSFLM (*18*). Data set Native-B was collected at a

Table 2: Refinement of Crystal Form B in Space Group *I*222

resolution (Å)	39−2.1
R-factor (R_{free}, 5% test set)	0.197 (0.263)
no. of unique reflections	28972
no. of non-H atoms	
protein	3762
sulfate	5
glycerol	6
solvent	216
average *B*-factor (Å^2)	23
rmsd for bond lengths (Å)	0.017
rmsd for bond angles (deg)	2.4
rmsd for *B*-factor along bonds (Å^2)	1.5
rmsd for *B*-factor along angles (Å^2)	2.2
Ramachandran quality (%)[a]	90/0

[a] Residues in the most-favored/disallowed regions of the ϕ and ψ diagram of backbone dihedral angles (*41*). The side chain dihedral angles χ_1 and χ_2 of Ile and Leu were fully in the expected ranges.

temperature of 100 K. For shock-freezing, the crystals were equilibrated with 20% (v/v) glycerol in the reservoir solution.

Structure Determination. Crystal form A was used for multiple isomorphous replacement (MIR)[1] phasing. For preparation of heavy atom derivatives, crystals were soaked with methylmercury acetate (MMA) and *cis*-$Pt(NH_3)_2Cl_2$ (CIP) for 2 days at concentrations of 20 mM. Four major heavy atom sites were located in the MMA difference Patterson map using the program SHELXS (*19*). All other sites were determined by difference Fourier maps. The heavy atom parameters were refined with MLPHARE (*18*), resulting in an overall figure of merit of 0.42 at 2.8 Å resolution.

A self-rotation function was calculated with the program POLARRFN (*18*) using data set Native-A (Table 1) in the Patterson range of 30−15 Å. Strong peaks in the section $\kappa = 180°$ at ω and φ values of 0.9° and 0°, and 90.9° and 0°, respectively, amounted to about 99% of those at the crystallographic 2-fold screw axis at ω and φ values of 90° and 90°, respectively. A local density correlation search with the program GETAX (*20*) was used to locate the three corresponding 2-fold axes within the unit cell. Density modification, including solvent flattening, histogram matching, and 4-fold noncrystallographic symmetry (NCS) averaging, was performed with the program DM (*18*, *21*).

Crystal form B was solved by molecular replacement using the refined molecular structure in crystal form A as a search model in the program AMoRe (*18*, *22*). The search was carried out in the resolution range from 10 to 6.5 Å with an outer radius of 33 Å, resulting in a single significant solution with a correlation coefficient of 72% and an *R*-factor of 33%. The highest incorrect solution was at 41 and 50%, respectively. After rigid body refinement with XPLOR (*23*), we minimized the effect of model bias by truncating the final solution to the 465 residues with real space density correlations above 0.85.

Model Building, Refinement, and Graphics. The graphics program O (*24*) was used for model building, for visual inspection of $2F_o - F_c$ and $F_o - F_c$ maps, and for model corrections. The refinement was started with the program XPLOR (*23*) and later continued with the program REFMAC (*18*, *25*). All observed data were used, and the bulk solvent correction of XPLOR was applied. After the protein model was completed, the solvent structure was elucidated with further cycles of REFMAC combined with ARPP (*18*, *26*).

[1] Abbreviations: MIO, 4-methylidene-imidazole-5-one; MIR, multiple isomorphous replacement; NCS, noncrystallographic symmetry; rmsd, root-mean-square deviation.

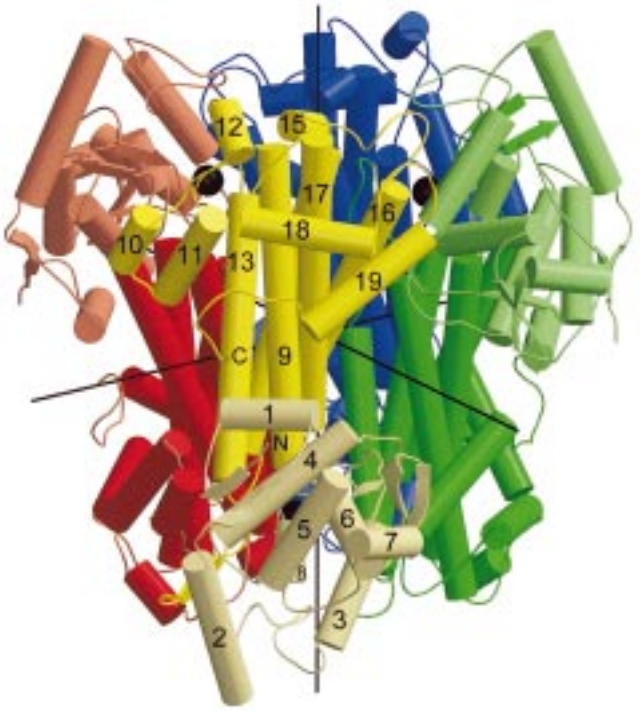

FIGURE 2: Histidase D_2 tetramer consisting of subunits A (green), B (red), C (yellow), and D (blue); black lines denote the three 2-fold axes. The N-terminal domains are depicted in lighter colors. The active centers are marked as black spheres.

The molecular model for the novel electrophilic group 4-methylidene-imidazole-5-one (MIO) was built under the assumption that protein atoms 142-C, 142-CA, 143-N, 143-CA, 143-CB, 143-C, 143-O, and 144-N are in one plane and that the double bonds are conjugated. The model was energy-minimized with SYBYL (version 1992, Tripos Associates Inc., St. Louis, MO) and included in the refinement.

Figures 1−3 and 6 were drawn using programs MOLSCRIPT (*27*) and Raster3D (*28*). The density map was produced using the program O (*24*). Solvent accessible surface areas were calculated with XPLOR (*23*) using a probe radius of 1.4 Å.

RESULTS AND DISCUSSION

Structure Elucidation. The crystallization of the wild-type histidase from *Ps. putida* (*13*) was hardly reproducible and yielded low-quality crystals at acidic pH, usually accompanied by protein precipitation (*16*, *29*). After observing unspecific aggregation under nonreducing conditions, we replaced Cys273 with alanine (*16*), which resulted in homogeneous preparations and high-quality crystals. The initially obtained crystal form A belongs to space group $P2_1$ ($a = 79.8$ Å, $b = 118.0$ Å, $c = 131.5$ Å, and $\gamma = 90.3°$) with one tetramer per asymmetric unit. It was used for MIR phasing (Table 1). On the basis of a self-rotation function (*18*) and a correlation search for 2-fold axes in a preliminary single isomorphous replacement electron density map (*20*), the noncrystallographic symmetry was established as D_2. The NCS-averaged electron density could be readily interpreted,

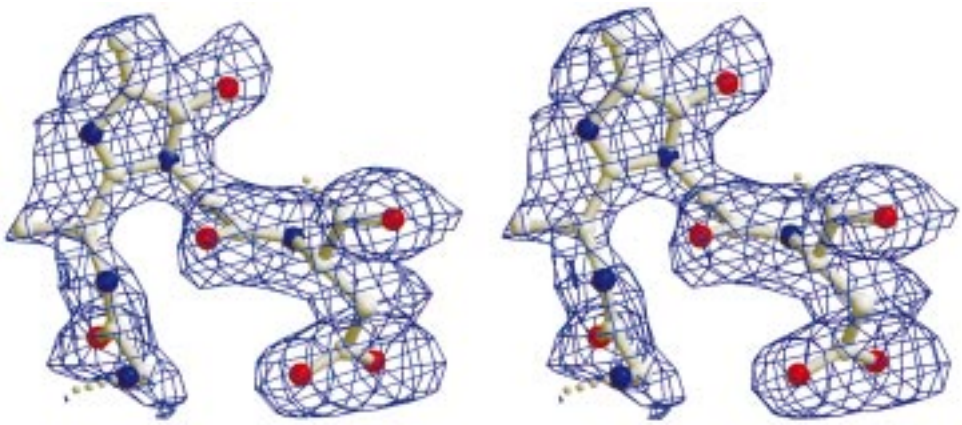

FIGURE 3: Stereoview of the prosthetic group MIO in its simulated-annealing $F_o - F_c$ omit electron density map (all depicted atoms were deleted) as contoured at 2.3σ. The chain cuts are dotted lines. To remove model bias, the protein model without MIO was run through a torsion slow cool procedure started at 1000 K (*23*) and subsequently refined again (*25*).

Table 3: Refined Geometry of the Catalytically Essential Electrophile MIO of Histidase

distance[a] (Å)		torsion angle[a]	
142-CA···142-C	1.54 (1.51)	142-CA···C···N···143-CA	168 (−178)
142-C···143-N	1.25 (1.26)	142-C···N···CA···143-C	0 (0)
143-N···143-CA	1.46 (1.43)	142-C···N···CA···143-CB	−179 (−179)
143-CA···143-CB	1.33 (1.34)	143-N···CA···C···144-N	0 (−2)
143-CA···143-C	1.45 (1.47)	143-N···CA···C···143-O	179 (177)
143-C···143-O	1.25 (1.22)	143-CA···C···N···142-C	−1 (3)
143-C···144-N	1.35 (1.34)	143-CA···C···N···144-CA	−125 (−118)
144-N···144-CA	1.50 (1.48)	143-C···N···C···143-N	0 (−3)
144-N···142-C	1.34 (1.34)	143-O···C···N···144-CA	55 (61)

[a] In parentheses are the starting values of MIO as constructed and energy-minimized with SYBYL.

yielding the complete model of the enzyme. Activity measurements of dissolved crystals showed, however, that the crystallized enzyme was inactive.

To obtain the structure of the active enzyme, we crystallized freshly prepared, fully active histidase and obtained crystal form B belonging to space group *I*222 (a = 79.3 Å, b = 116.8 Å, and c = 129.5 Å) with one subunit in the asymmetric unit. Dissolved form B crystals showed an enzymatic activity at the usual level. Data for crystal form B were collected to a resolution of 2.1 Å (Table 1), and the structure was solved by molecular replacement using the model from crystal form A. The structure was refined to an R-factor of 19.7% (R_{free} = 26.3%) with satisfying stereochemistry (Table 2).

The packing arrangements in the two crystal forms resemble each other closely. In crystal form A ($P2_1$), the molecular 2-fold axes are local, and they deviate 1.9° from the y-axis and about 6° each from the x- and z-axes. In crystal form B, they are crystallographic and coincide with the respective axes. The enzyme structures in crystal forms A and B are closely similar, and the root-mean-square deviation (rmsd) of all atoms is 0.58 Å. Significant differences occur only at the mobile surface loops around residues 62, 272, 370, and 407. The inactive enzyme in crystal form A showed additional density at the C_β atom of residue 143, which was originally a serine. This density probably indicates a partial hydroxylation of the electrophilic group. All following descriptions and discussions refer to the active enzyme structure in crystal form B.

Histidase Architecture and Topology. Histidase from *Ps. putida* is a homotetramer exhibiting D_2 symmetry with 509 amino acid residues (M_r = 53 593) per subunit. The chain

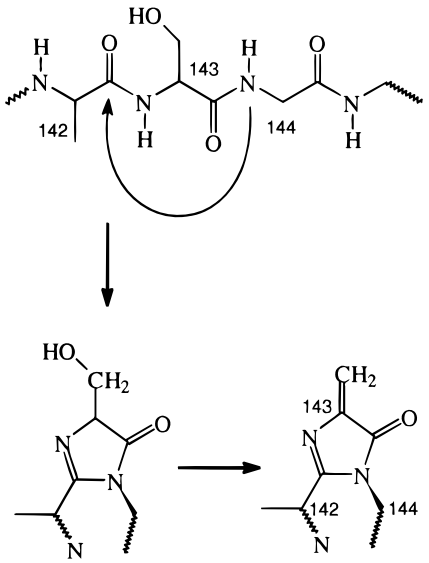

FIGURE 4: Proposed autocatalytic formation of MIO by two water elimination steps from the tripeptide Ala-Ser-Gly at positions 142−144. The refined MIO geometry is given in Table 3.

fold consists mainly of α-helices and can be subdivided into two domains (Figure 1). The 198 N-terminal residues constitute a globular domain of eight helices and four short β-strands. The C-terminal domain consists of a core of five long, nearly parallel α-helices (α9, α13, α14, α16, and α17) that is surrounded by six further helices (α10, α11, α12, α15, α18, and α19). The helix arrangement gives the subunit a dumbbell shape. In the D_2 tetramer, the five-helix bundles of the C-terminal domains assemble to form a central core of 20 nearly parallel α-helices (Figure 2). The association

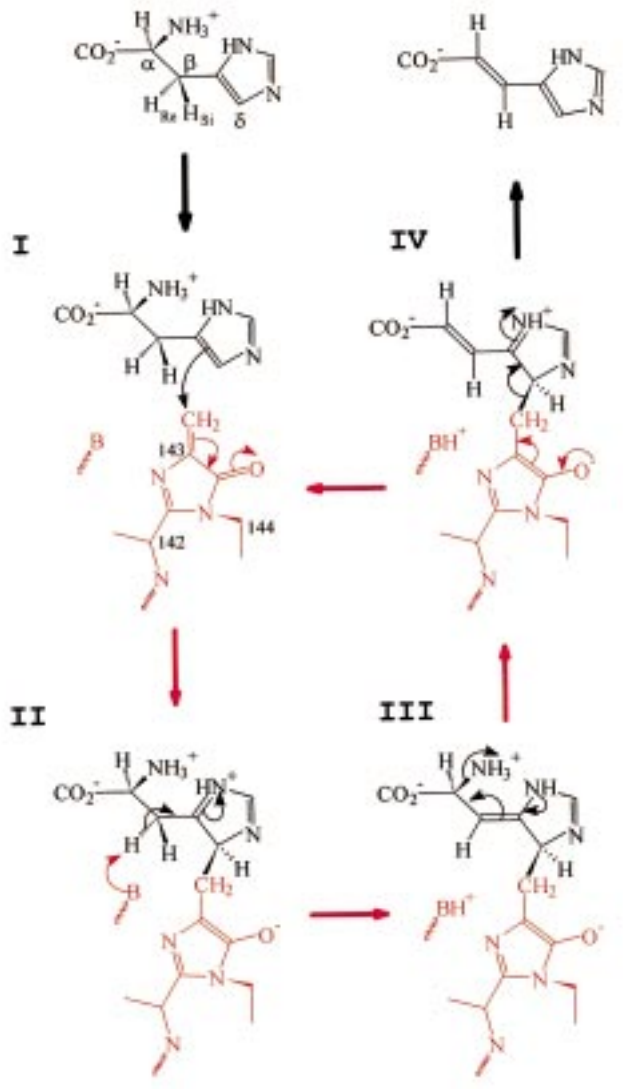

FIGURE 5: Proposed mechanism of histidase action as adapted from ref *3*. (I) The novel electrophilic prosthetic group 4-methylidene-imidazole-5-one (MIO) in the active center (red) forms a covalent intermediate with the substrate histidine (black). (II) The C_β protons are activated, and H_{Re} is abstracted by an enzymatic base. (III) Ammonia is eliminated. (IV) The enzyme regenerates by releasing the product urocanate.

buries a total of 32% of the solvent-accessible surface (27 200 Å^2) in the interfaces between subunits A and B (261 Å^2) and A and C (2961 Å^2), as well as between A and D (3578 Å^2).

The chain fold topology is similar (*30*) to that of a family of tetrameric enzymes catalyzing the elimination of various groups from carboxylic acids, as for instance a hydroxyl by fumarase (*31*), ammonia by aspartase (*32*), or a guanidino group by argininosuccinate lyase (*33*). The avian eye lens protein *δ*-crystallin also belongs to this family as an inactive form of the latter enzyme (*34*). None of the sequences of these proteins is detectably homologous to histidase or phenylalanine ammonia-lyase.

Active Center. The active center of histidase has been located by combining information from sequence data, mutations, and mechanism-based labeling studies. Each of the four active centers of the tetramer is formed by residues from three different subunits; the reference subunit (e.g., A) provides residues ^{A}53−59, ^{A}79−84, ^{A}141−147, and ^{A}191−197 from the N-terminal domain and residues ^{A}311−330 and ^{A}409−417 from the C-terminal domain. Subunits C and D add residues ^{C}382 and ^{C}383 and ^{D}280−284, respectively. The access to the active center is narrowed by a mobile loop formed by residues ^{A}56−68 (Figure 1B).

It has been proposed that at position 143 (*35*) the enzyme uses a dehydroalanine derived from a serine as an electrophile (*8*, *9*). In both crystal forms, however, the observed electron density around residue 143 was inconsistent with a dehydroalanine and any of the standard amino acids. In particular, it does not account for the carbonyl oxygen of Ala142. The density is in excellent agreement, however, with a 4-methylidene-imidazole-5-one (MIO) group (Figure 3), which can be formed by two water elimination steps from the internal tripeptide Ala-Ser-Gly at positions 142−144 (Figure 4). The first step is a cyclization−elimination by an intramolecular nucleophilic attack of the nitrogen of Gly144 at the carbonyl group of Ala142. A subsequent water elimination from the side chain of Ser143 completes the system of cross-conjugated double bonds. The detailed geometry of refined MIO is given in Table 3. As the C_α−N bond at position 144 was clearly running out of this plane (the angle O−C−N−C_α is 54°), the N atom at this position is sp^3-hybridized. The

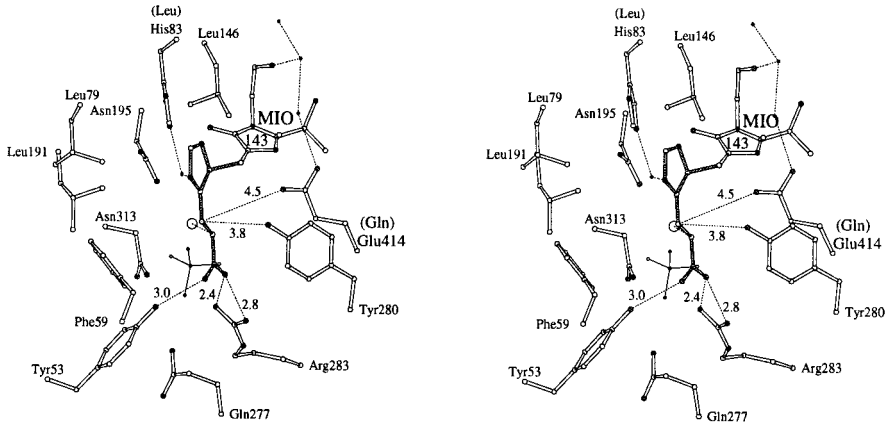

FIGURE 6: Stereoview of the active center with the modeled intermediate (gray) corresponding to state IV in Figure 5. The residues of this figure are conserved in histidases and, except for His83 and Glu414, also in phenylalanine ammonia-lyases (residues in parentheses). The bound sulfate ion from the crystallization buffer (thin lines) and four water molecules (dots) are shown. The amino group position of histidine is indicated (○). Dotted lines denote putative interactions with distances in angstroms. The overall fit of the model is tight, indicating that movements in the range of 1 Å occur during catalysis.

resulting electrophilic group MIO can be regarded as a modified dehydroalanine whose electrophilicity is enhanced by preventing delocalization of the nitrogen lone pairs of residues 143 and 144 into the α,β-unsaturated carbonyl system (Figure 4).

Electrophile MIO. The formation of MIO proceeds most likely autocatalytically, because heterologous expression of various pro- and eukaryotic histidase genes in *E. coli* (*8*, *14*) and in COS-cells (*36*) resulted in fully active enzymes. The first step of the reaction resembles the cyclization observed with the green fluorescent protein (GFP) (*37*, *38*). The driving force for the condensation reaction is not clear. A mechanical packing pressure is unlikely because both GFP and histidase have large water-filled cavities close to the modified peptide. A closer inspection of the environments of the two prosthetic groups showed no conspicuous similarities in the surrounding molecular groups.

The interpretation of the observed density as the novel electrophilic group MIO is consistent with mutagenesis studies and chemical modification experiments. The mutation of Ser143 to alanine or glycine, which cannot be converted to the methylidene group, abolished the activity. In contrast, a change to cysteine, from which the thiol group can be eliminated, resulted in a fully active enzyme with kinetics that are indistinguishable from those of the wild type (*9*). Corresponding mutations in a eukaryotic homologue (*36*) and in phenylalanine ammonia-lyase from parsley (*4*) gave similar results. Moreover, chemical inactivation experiments performed with NaB^3H_4 or $K^{14}CN$ with subsequent acid hydrolysis yielded [^{3}H]alanine (*6*) or [^{14}C]aspartate (*39*), respectively. All these results are consistent with both a dehydroalanine and MIO, but only MIO explains why an Edman degradation stopped two residues before Ser143 (*35*). Moreover, in an early chemical modification experiment with nitro[^{14}C]methane, the ene-imine moiety of MIO had been detected (*7*). Because MIO has the quality of an added organic compound, we propose to call it a prosthetic group, although it is a polypeptide modification.

Mechanism of Action. The reaction mechanism has been the subject of various experiments and discussions (*3*, *7*, *35*, *40*) resulting in the following proposal. Once histidine is bound to the enzyme, its C_δ atom attacks MIO at its methylidene function (Figure 5, state I). The positive charge introduced at the imidazole acidifies the protons at the C_β atom and also accounts for the observed hydrogen−deuterium exchange at the C_δ atom (*40*). After abstraction of the H_{Re} proton from C_β by an enzymatic base (state II), the α-ammonium group is eliminated (state III), and the product urocanate is released (state IV).

Because the available conformations of the intermediate urocanate−enzyme complex (state IV of Figure 5) are very limited, we have built it as a model in Figure 6. The only rotatable bonds are in the covalent link to MIO. The torsion angle around the C_β−C_γ bond of urocanate can be 0° or 180°, and the C_δ atom is chiral. In the crystal structure, a sulfate ion from the crystallization buffer is bound to Arg283, which is the only positively charged group in this region. We therefore placed the carboxylate of histidine at the sulfate position, where it forms a salt bridge with Arg283 and a hydrogen bond with Tyr53. Under this assumption, the C_δ atom must have (*S*)-configuration and the rotations around the two bonds are restricted to a small range, the center of which is displayed in Figure 6. The bound educt histidine has more degrees of freedom, but it occupies most likely a closely related position such that the α-amino group can be placed at a position where it interacts with Asn195 (Figure 6). Glu414 and Tyr280 are in suitable positions for deprotonating the C_β atom. A chain of water molecules extending to the bulk solvent could act as a proton relay. In conclusion, the model explains the essentials of the reaction and provides a promising basis for further exploring the unusual mechanism of this important group of enzymes.

ACKNOWLEDGMENT

We thank M. Langer and M. Bädeker for help at early stages of the project as well as C. Vonrhein and J. E. W. Meyer for discussions.

REFERENCES

1. Morrison, H., Bernasconi, C., and Pandey, G. (1984) *Photochem. Photobiol. 40*, 549−550.
2. Taylor, R. G., Levy, H. L., and McInnes, R. R. (1991) *Mol. Biol. Med. 8*, 101−116.
3. Langer, M., Pauling, A., and Rétey, J. (1995) *Angew. Chem., Int. Ed. 34*, 1464−1465.
4. Schuster, B., and Rétey, J. (1995) *Proc. Natl. Acad. Sci. U.S.A. 92*, 8433−8437.
5. Hahlbrock, K., and Scheel, D. (1989) *Annu. Rev. Plant Physiol. Plant Mol. Biol. 40*, 347−369.
6. Wickner, R. B. (1969) *J. Biol. Chem. 244*, 6550−6552.
7. Givot, I. L., Smith, T. A., and Abeles, R. H. (1969) *J. Biol. Chem. 244*, 6341−6353.
8. Langer, M., Reck, G., Reed, J., and Rétey, J. (1994) *Biochemistry 33*, 6462−6467.
9. Langer, M., Lieber, A., and Rétey, J. (1994) *Biochemistry 33*, 14034−14038.
10. Sahl, H. G., Jack, R. W., and Bierbaum, G. (1995) *Eur. J. Biochem. 230*, 827−853.
11. Volkin, D. B., and Klibanov, A. M. (1987) *J. Biol. Chem. 262*, 2945−2950.
12. Ohmiya, Y., Hayashi, H., Kondo, T., and Kondo, Y. (1990) *J. Biol. Chem. 265*, 9066−9071.
13. Consevage, M. W., and Phillips, A. T. (1990) *J. Bacteriol. 172*, 2224−2229.
14. Hernandez, D., and Phillips, A. T. (1993) *Protein Expression Purif. 4*, 473−478.
15. Tabor, H., and Mehler, A. H. (1955) *Methods Enzymol. 2*, 228−233.
16. Schwede, T. F., Bädeker, M., Langer, M., Rétey, J., and Schulz, G. E. (1999) *Protein Eng. 12*, 151−153.
17. Kabsch, W. (1988) *J. Appl. Crystallogr. 21*, 916−924.
18. Collaborative Computing Project, Number 4 (1994) *Acta Crystallogr. D 50*, 760−763.
19. Sheldrick, G. M., Dauter, Z., Wilson, K. S., Hope, H., and Sieker, L. C. (1993) *Acta Crystallogr. D 49*, 18−23.
20. Vonrhein, C., and Schulz, G. E. (1999) *Acta Crystallogr. D 55*, 225−229.
21. Cowtan, K. D., and Main, P. (1996) *Acta Crystallogr. D 52*, 43−48.
22. Navaza, J. (1994) *Acta Crystallogr. A 50*, 157−163.
23. Brünger, A. T. (1993) *X-PLOR Version 3.1. A system for X-ray crystallography and NMR*, Yale University Press, New Haven.
24. Jones, T. A., Zou, J.-Y., Cowen, S. W., and Kjeldgaard, M. (1991) *Acta Crystallogr. A 47*, 110−119.
25. Murshudov, G. N., Vagin, A. A., and Dodson, E. J. (1997) *Acta Crystallogr. D 53*, 240−255.
26. Lamzin, V. S., and Wilson, K. S. (1993) *Acta Crystallogr. D 49*, 129−147.
27. Kraulis, P. J. (1991) *J. Appl. Crystallogr. 24*, 946−950.
28. Merritt, E. A., and Bacon, D. J. (1997) *Methods Enzymol. 277*, 505−524.

29. Teo, B., Kidd, R. D., Mack, J., Tiwari, A., Hernandez, D., Phillips, A. T., and Farber, G. K. (1998) *Acta Crystallogr. D 54*, 681−683.
30. Holm, L., and Sander, C. (1993) *J. Mol. Biol. 233*, 123−138.
31. Weaver, T. M., Levitt, D. G., Donnelly, M. I., Wilkens-Stevens, P. P., and Banaszak, L. J. (1995) *Nat. Struct. Biol. 2*, 654−662.
32. Shi, W., Dunbar, J., Jayasekera, M. M. K., Viola, R. E., and Farber, G. K. (1997) *Biochemistry 36*, 9136−9144.
33. Turner, M. A., Simpson, A., McInnes, R. R., and Howell, P. L. (1997) *Proc. Natl. Acad. Sci. U.S.A. 94*, 9063−9068.
34. Simpson, A., Moss, D., and Slingsby, C. (1995) *Structure 3*, 403−412.
35. Hernandez, D., Stroh, J. G., and Phillips, A. T. (1993) *Arch. Biochem. Biophys. 307*, 126−132.
36. Taylor, R. G., and McInnes, R. R. (1994) *J. Biol. Chem. 269*, 27473−27477.
37. Ormö, M., Cubitt, A. B., Kallio, K., Gross, L. A., Tsien, R. Y., and Remington, S. J. (1996) *Science 273*, 1392−1395.
38. Reid, B. G., and Flynn, G. C. (1997) *Biochemistry 36*, 6786−6791.
39. Consevage, M. W., and Phillips, A. T. (1985) *Biochemistry 24*, 301−308.
40. Furuta, T., Takahashi, H., Shibasaki, H., and Kasuya, Y. (1992) *J. Biol. Chem. 267*, 12600−12605.
41. Laskowski, R. A., MacArthur, M. W., Moss, D. S., and Thornton, J. M. (1993) *J. Appl. Crystallogr. 26*, 283−291.

BI982929Q